Damage detection of metro tunnel structure through transmissibility function and cross correlation analysis using local excitation and measurement

Lei FENG [1,2,3], Xiaohua YI [2], Dapeng ZHU[2], Xiongyao XIE*[1, 3], Yang WANG[2]

[1] Department of Geotechnical Engineering, College of Civil Engineering, Tongji University, 1239 Siping Road, Shanghai, P.R. China

[2] School of Civil and Environmental Engineering, Georgia Institute of Technology 790 Atlantic Dr NW, Atlanta, GA, USA

[3] Key Laboratory of Geotechnical & Underground Engineering of Ministry of Education, Tongji University, 1239 Siping Road, Shanghai, P.R. China

*xiexiongyao@tongji.edu.cn ; phone 86-13501782144; fax 86-21-65983479

Abstract: In a modern metropolis, metro rail systems have become a dominant mode for mass transportation. The structural health of a metro tunnel is closely related to public safety. Many vibration-based techniques for detecting and locating structural damage have been developed in the past several decades. However, most damage detection techniques and validation tests are focused on bridge and building structures; very few studies have been reported on tunnel structures. Among these techniques, transmissibility function and cross correlation analysis are two well-known diagnostic approaches. The former operates in frequency domain and the latter in time domain. Both approaches can be applied to detect and locate damage through acceleration data obtained from sensor arrays. Furthermore, the two approaches can directly utilize structural response data without requiring excitation measurement, which offers advantages in field testing on a large structure. In this research, a numerical finite element model of a metro tunnel is built and different types of structural defects are introduced at multiple locations of the tunnel. Transmissibility function and cross correlation analysis are applied to perform structural damage detection and localization, based on simulated structural vibration data. Numerical results demonstrate that the introduced defects can be successfully identified and located. The sensitivity and feasibility of the two approaches have been verified when sufficient distribution of measurement locations is available. Damage detection results of the two different approaches are compared and discussed.

Keywords: Structural health monitoring; damage detection; metro tunnel; transmissibility function; cross correlation.

1. Introduction

In modern international metropolis such as New York City, Shanghai, or Tokyo, urban population has reached tens of millions. As a result, ground transportation has become increasingly insufficient for satisfying public commuting demands, while the metro system has become preferred by many for daily commuting. The health of metro tunnel structures is of significant importance to public safety. However, due to harsh operational and environmental conditions, metro tunnel structures may gradually deteriorate and require timely maintenance over the service life [1].

In the past decades, structural health monitoring systems have been widely adopted to monitor the behavior of structures and evaluate the safety and durability of structures. Structural health monitoring system has been progressively regarded as an effective way to reduce risks for underground structures [2]. Many damage identification techniques for detecting and locating existing damage have been developed recently, and many algorithms aim to identify damage using changes in structural vibration [3,4]. The main presumption of using vibration data is that the existence of damage changes structural stiffness, and thus changes structural modal properties that can be extracted from vibration test [5]. Following recent rapid developments in metro tunnel engineering, vibration-based structural health monitoring approach for tunnel-soil coupled system was researched. A Timoshenko beam-Transfer Matrix Method is developed to determine the relationship between the tunnel Young's modulus and the coupled resonance frequency [6]. A structural health assessment method based on torsional wave speed was proposed to determine the tunnel structure's global stiffness, and evaluate the tunnel's structural service status further [7]. Damage identification algorithms based on vibration data can provide information regarding the overall health condition of the structure, and vibration test is relatively low-cost to implement in the field.

Vibration-based damage identification techniques can be categorized into two groups: model-based approaches and non-model-based approaches [4]. Model-based approaches assume that structural response can be accurately simulated with numerical models such as FEM (finite element model). If the numerical model fails to accurately reflect the response of structure in the field, the performance in damage detection suffers. Alternatively, non-model-based approaches may avoid such difficulties and demonstrate advantages in large-scale structures. The reason lies in the challenge of acquiring an accurate finite element model for large-scale structures, even when field measurement data is available for updating and calibrating the model. Among various non-model approaches, transmissibility function and cross correlation analysis are both capable of structural damage detection and localization. Both approaches can directly utilize structural response data (without excitation measurement), which offers advantages in large structure testing.

Both theoretical development and field application using transmissibility function for damage detection and localization have been investigated by researchers. The transmissibility relationship between frequency response functions was considered by Liu and Ewins [8], where transmissibility

function was defined as the ratio of frequency response functions for a chain-like multi-degree-of-freedom system. A more generalized transmissibility concept was proposed by [9] as a powerful tool for modal analysis. Translational and curvature transmissibility functions were adopted to detect and locate damage on a cantilever beam by [10]. The research demonstrated that more accurate damage detection could be achieved when high frequency range of the transfer function is used. In addition, transmissibility function were analytically derived by [11] for detecting and locating damage in linear and nonlinear structures. Two damage detection cases, a representative three-story building structure and a rotorcraft fuselage, were later applied with transmissibility function analysis by [12] , where reliable damage detection was obtained in spite of certain environmental fluctuations and non-linearity in boundary condition. The work by [13] demonstrated that transmissibility function analysis was able to detect a single bolt loosening with reduced tightening torque. Furthermore, the influence of operational and environmental variability on the damage indicator were analyzed by [14] . The results showed that the accuracy and reliability of transmissibility function analysis could be improved by identifying specific frequency ranges that are more sensitive to damage and immune to sources of variability. More recently, Yi and Zhu [15,16] developed a mobile sensing system which is capable of maneuvering on the surface of ferromagnetic materials. Transmissibility function analysis was embedded in mobile sensing nodes; using data collected by mobile sensing nodes, on-board computation was successfully conducted to detect damage on a steel frame.

On the other hand, cross correlation analysis has also been studied by many researchers in the last few decades. [17] proposed that cross correlation functions between two response signals under ambient excitation have the same waveform as impulse response functions. The resonance frequencies and modal damping of the structure were estimated from cross correlation functions. The Hilbert-Huang transform of cross correlation functions was studied by [18]. The stiffness and damping coefficients of Phase-I IASC-ASCE benchmark building were identified; damage locations and severities can be identified by comparing stiffness prior to and after damage. Furthermore, a damage indicator was proposed by [19]. The indicator was defined by comparing the peak amplitude of the cross correlation function of the damaged structure versus that of the undamaged structure. Laboratory experiments on a steel portal frame were conducted to validate the damage detection approach. A prerecorded catalog of Green's function templates and a cross-correlation method was recently proposed by Heckman; brittle fracture of welded beam-column connections in steel moment-resisting frames (MRFs) was detected by using proposed method [20].

In most applications, transmissibility function and cross correlation analysis were applied to data acquired on beams, plates, frames and multistory building models. Little research has been reported on the application on underground structures. This paper describes the application of these two approaches on diagnosing damage in an underground metro tunnel. In this study, a numerical model of a metro tunnel structure is established with consideration of soil constraints. Different types of structural defects are introduced at multiple locations of the tunnel. Transmissibility function and cross correlation analysis are applied to perform structural damage detection and localization.

2. Transmissibility function and cross correlation algorithms

Damage detection algorithms based on transmissibility function and cross correlation analysis are briefly reviewed in Sections 2.1 and 2.2, respectively.

2.1. Transmissibility function algorithm

The forced vibration of a viscously damped *n*-degree-of-freedom (DOF) system is governed by:

$$\mathbf{M}\ddot{\mathbf{x}}(t)+\mathbf{C}\dot{\mathbf{x}}(t)+\mathbf{K}\mathbf{x}(t)=\mathbf{f}(t) \tag{1}$$

where **x**(t) is the $n\times1$ displacement vector, and **f**(t) is the $n\times1$ external force vector, and **M**, **C**, **K** are respectively the mass, damping, and stiffness matrices. If external force is only applied to the *k*-th DOF, vector **f**(t) has only one non-zero entry, i.e. $\mathbf{f}(t)=\{0_1,0_2,\ldots,f_k(t),\ldots,0_n\}^{\mathrm{T}}$.

Through Fourier transform, Eq. (1) can be represented in frequency domain as

$$\mathbf{X}(\omega)=\mathbf{H}(\omega)\mathbf{F}(\omega) \tag{2}$$

where $\mathbf{H}(\omega)$ is the $n\times n$ frequency response function (FRF) matrix. Assuming external force is only applied to the *k*-th DOF, the Fourier transform of the external force vector $\mathbf{f}(t)$ is determined as

$$\mathbf{F}(\omega)=\{0_1,0_2,\ldots,F_k(\omega),\ldots,0_n\}^{\mathrm{T}} \tag{3}$$

The acceleration vector in frequency domain can be computed from Eq. (2) as

$$\mathbf{A}(\omega)=-\omega^2\mathbf{H}(\omega)\mathbf{F}(\omega) \tag{4}$$

The transmissibility function $T_{ij}(\omega)$ between output DOFs *i* and *j* is defined as the ratio between two frequency spectra, $A_i(\omega)$ and $A_j(\omega)$. Let $\mathbf{h}_i^{\mathrm{T}}(\omega)$ be the *i*-th row of $\mathbf{H}(\omega)$, $\mathbf{h}_j^{\mathrm{T}}(\omega)$ be the *j*-th row of $\mathbf{H}(\omega)$, the transmissibility function $T_{ij}(\omega)$ can be calculated as

$$T_{ij}(\omega)=\frac{A_i(\omega)}{A_j(\omega)}=\frac{-\omega^2\mathbf{h}_i^{\mathrm{T}}(\omega)\mathbf{F}(\omega)}{-\omega^2\mathbf{h}_j^{\mathrm{T}}(\omega)\mathbf{F}(\omega)}=\frac{\mathbf{h}_i(\omega)^{\mathrm{T}}\mathbf{F}(\omega)}{\mathbf{h}_j(\omega)^{\mathrm{T}}\mathbf{F}(\omega)} \tag{5}$$

Substituting $\mathbf{F}(\omega)$ in Eq. (3) into Eq. (5), $T_{ij}(\omega)$ is further simplified as

$$T_{ij}(\omega)=\frac{H_{ik}(\omega)}{H_{jk}(\omega)} \tag{6}$$

where $H_{ik}(\omega)$ and $H_{jk}(\omega)$ are entries of the FRF/receptance matrix. Although Eq. (6) helps to demonstrate that the transmissibility function $T_{ij}(\omega)$ is an inherent structural property determined by

the receptance matrix, it should be noted that practical calculation of the transmissibility function doesn't require the two receptance entries. Instead, the calculation can be based upon the basic definition of the transmissibility function $T_{ij}(\omega)$, as shown by the first equal sign of Eq. (5). In other words, practical calculation of $T_{ij}(\omega)$ only involves the two response spectra $A_i(\omega)$ and $A_j(\omega)$, without requiring the measurement of the excitation force or the calculation of receptance entries.

Transmissibility damage indicator (*TDI*) between DOFs *i* and *j* is defined as

$$TDI_{ij} = \frac{\int_{\omega_1}^{\omega_2} \left| \log\left|T_{ij}^{U}\right| - \log\left|T_{ij}^{D}\right| \right| d\omega}{\int_{\omega_1}^{\omega_2} \left| \log\left|T_{ij}^{U}\right| \right| d\omega} \tag{7}$$

where ω_1 and ω_2 are the lower and upper bounds of the interested frequency span, superscript *U* represents the undamaged structure, and superscript *D* represents the damaged structure. Accordingly, T_{ij}^{U} represents the transmissibility function of the undamaged structure, and T_{ij}^{D} represents the transmissibility function of the damaged structure. The transmissibility damage indicator *TDI* is defined in logarithmic scale to emphasize the effect of overall waveform difference, while suppressing the effect of occasional sharp peaks in the transmissibility functions that may occur in practice.

2.2 Cross correlation algorithm

Considering the forced response of the aforementioned *n*-DOF system, the deterministic cross correlation function between the acceleration response at the *i*-th and *j*-th DOFs is given by:

$$R_{ij}(\tau) = \lim_{T\to\infty} \frac{1}{T} \int_0^T \ddot{x}_i(t)\ddot{x}_j(t+\tau)\,dt \tag{8}$$

Where τ is the time lag, $\ddot{x}_i(t)$ and $\ddot{x}_j(t)$ represent the acceleration response at DOFs *i* and *j*, respectively. The time-discretized version of the cross-correlation function is defined as:

$$R_{ij}(k) = \begin{cases} \dfrac{1}{N-k} \displaystyle\sum_{n=0}^{N-k-1} \ddot{x}_i(n+k)\ddot{x}_j(n), & k \geq 0 \\ R_{ji}(-k), & k < 0 \end{cases} \tag{9}$$

where *N* denotes the length of the measurement data. The deterministic cross correlation function can be normalized by:

$$\tilde{R}_{ij}(k) = \frac{R_{ij}(k)}{\sqrt{R_{ii}(0)}\sqrt{R_{jj}(0)}} \tag{10}$$

Under impact excitation, cross correlation functions are determined by the impulse responses that correspond to inherent dynamic properties of the structure. Therefore, damage can be identified by comparing the cross correlation functions of the undamaged structure and damaged structure. In this

work, integral of normalized deterministic cross correlation functions are used for comparison, which is denoted as the cross-correlation damage indicator CDI_{ij}:

$$CDI_{ij} = \frac{\sum_{k_1}^{k_2} \left\| \left| \tilde{R}_{ij}^{D} \right| - \left| \tilde{R}_{ij}^{U} \right| \right\|}{\sum_{k_1}^{k_2} \left| \tilde{R}_{ij}^{U} \right|} \tag{11}$$

where superscripts U and D represent the undamaged structure and the damaged structure, respectively; $\tilde{R}_{ij}^{U}$ represents the normalized cross correlation function of undamaged structure; and $\tilde{R}_{ij}^{D}$ represents the normalized cross correlation function of damaged structure.

3. Numerical simulation of a metro tunnel structure

To validate the feasibility and sensitivity of proposed damage detection approaches, a metro tunnel structure with soil constraints is constructed in ANSYS. Structural vibration response data is obtained before and after introducing different types of damage to the tunnel model. This section describes the numerical model, as well as the excitation and measurement schemes for collecting response data.

3.1 Numerical model

Fig. 1(a) shows the finite element model of a metro tunnel structure in ANSYS software. The tunnel structure is discretized using SHELL181 element. Listed in Table 1, the concrete material properties adopted in this model are the average values from material testing for the Shanghai metro tunnel. To eliminate the effect of boundary condition, longitudinal dimension of the tunnel is set to 168m, and the element length is 1.2m. Modal damping of 3% is assigned to each vibration mode. Section dimensions are also consistent with the Shanghai metro tunnel, where the outer diameter is 6.2m, inner diameter is

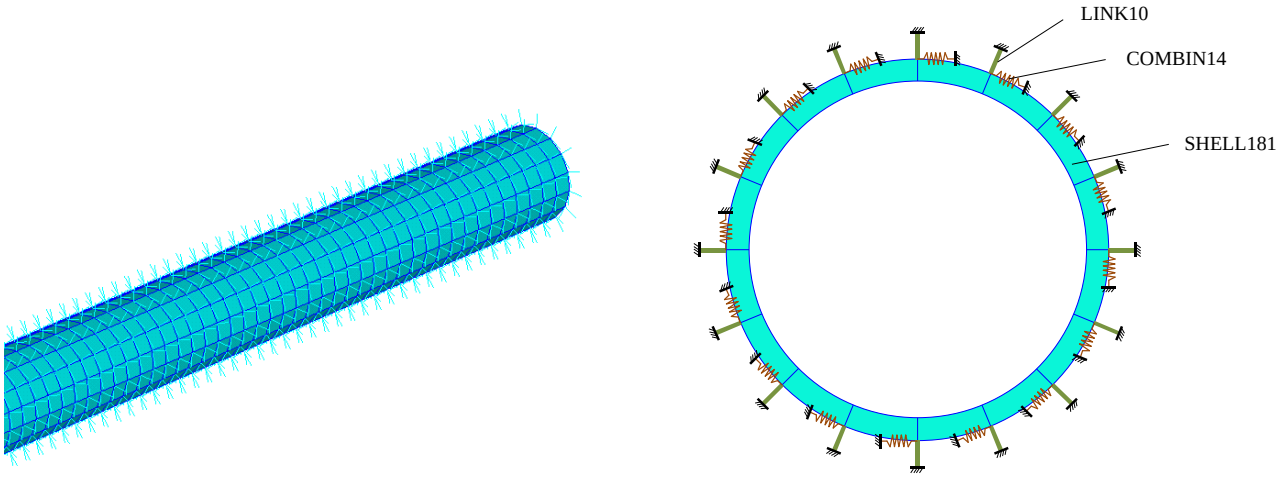

(a) (b)

Fig. 1. (a) Finite element model of the tunnel structure with soil constraints; (b) Section and ground constraint modeling

5.5m, and tunnel wall thickness is 0.35m. The entire cross section circumference is divided into 16 elements (as shown in Fig. 1(b)).

Average soil properties around the Shanghai metro tunnel are shown in Table 1. Soil constraints around the tunnel structure are simulated with full-circle ground spring hypothesis. Soil does not permit the development of tensile stress. Therefore, as shown in Fig. 1 (b), sixteen compression-only LINK10 elements are adopted to model the ground reactions in radial direction, and sixteen uniaxial tension-compression COMBIN14 elements are adopted in tangential direction. Coefficients of these two element types are calculated according to elastic theory [21,22], corresponding elastic modulus of LINK10 element and COMBIN14 element are listed in Table 1.

Table 1: Material properties

Material	Elastic modulus (MPa)	Poisson's ratio	Density (kg/m^3)	Spring constant (N/m)
Concrete	3.45×10^4	0.2	2,551	-
Soil	5.0	0.3	1,836	-
LINK10	5.06×10^2	-	-	-
COMBIN14	-	-	-	3.0×10^6

3.2. Excitation and measurement procedure in metro tunnel model

As shown in Fig. 2, a total of thirteen excitation and measurement points at tunnel bottom are allocated along the longitudinal direction, with a spacing of 12m (i.e. ten tunnel element lengths). For obtaining vibration data, a simulated impact excitation is sequentially applied to each point. An ideal impulse is applied as excitation input. The excitation magnitude is set as 30 KN, based on potential modal hammers available in the market. Since the vibration signal attenuates with increased distance from the excitation, radial acceleration data at only two locations adjacent to the excitation are collected. In detail, when excitation is applied at location i+1 ($1 \le i \le 12$) respectively, corresponding acceleration data is collected at location pairs i and (i+1). Considering the limitation of hardware performance in future field tests, the sampling frequency is set to 2,500 Hz, and the duration for each acceleration measurement is five seconds. After each impact excitation, the vibration decays within about 0.1 second. For example, Fig. 3 shows truncated acceleration time history at locations 4 and 5 when an impact excitation is applied at location 5. It should be noted that such a local excitation and

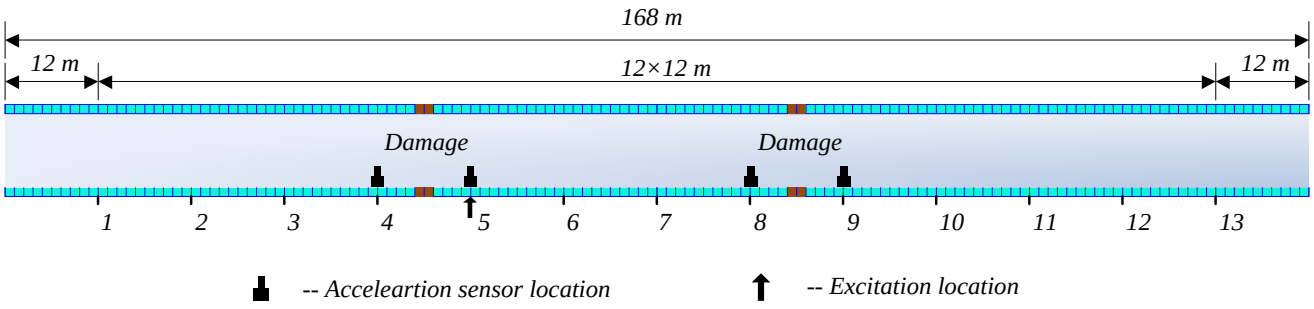

Fig. 2. Simulated impact excitation and corresponding two acceleration measurement locations

measurement scheme is convenient to execute in practical field testing.

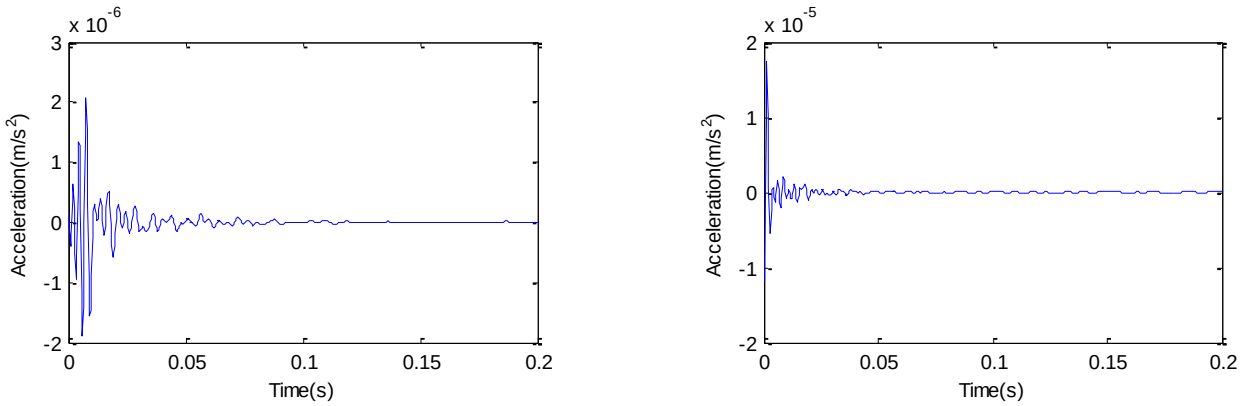

(a) (b)

Fig. 3. Truncated acceleration time history when an impact excitation is located at location 5: (a) Acceleration time history at location 4; (b) Acceleration time history at location 5

4. Damage detection results through transmissibility function and cross correlation analysis

This section investigates the feasibility and sensitivity for damage detection, using both transmissibility function and cross correlation analysis. Different types of damage and severities are studied. Using acceleration data, damage identification procedures described in Section 2 are applied to calculate the transmissibility-function damage indicator (*TDI*) and cross-correlation damage indicator (*CDI*). In transmissibility function analysis, it is well known that the frequency range $\omega_1 \sim \omega_2$ shown in Eq. (7) has notable effect on the accuracy of damage identification [4,10,14]. In reality, damage typically is a local phenomenon, such as cracks or corrosion. Since higher frequency modes tend to capture local response, transmissibility functions at higher frequency range usually provide more accurate damage identification results. In this study, to cover high frequency range, the upper bound is set to 1000Hz, slightly lower than the Nyquist frequency, and a broad frequency range of 200 ~ 1,000Hz is used in the *TDI* calculation. Using the tunnel model introduced in Section 3, artificial damage is introduced by reduction in elastic modulus and tunnel wall thickness.

4.1. Elastic modulus reduction

This section studies the damage detection performance of transmissibility function and cross-correlation algorithm under elastic modulus reduction. Reduction of elastic modulus to the 16-element 2.4m-long ring segment between locations 4 and 5 is first studied. Different degrees of reduction are introduced, including 3%, 5%, 7%, 9%, 11%, 13%. In each damage scenario, the impact

load is sequentially applied at locations 2, 3, …, and 13. Correspondingly, acceleration records are respectively collected at location pairs 1-2, 2-3, …, and 12-13.

4.1.1. Transmissibility function

For all different degrees of elastic modulus reduction scenarios, the magnitude of transmissibility functions between location pairs 1-2, 4-5, and 12-13 are illustrated in Fig. 4. To clearly demonstrate the differences among multiple damage scenarios, the plots are zoomed in to a smaller frequency range. Compare with location pairs 1-2 and 12-13, damage-caused change can be observed in transmissibility function at pair 4-5. In addition, for transmissibility function at pair 4-5, it is obvious that more severe damage causes more change.

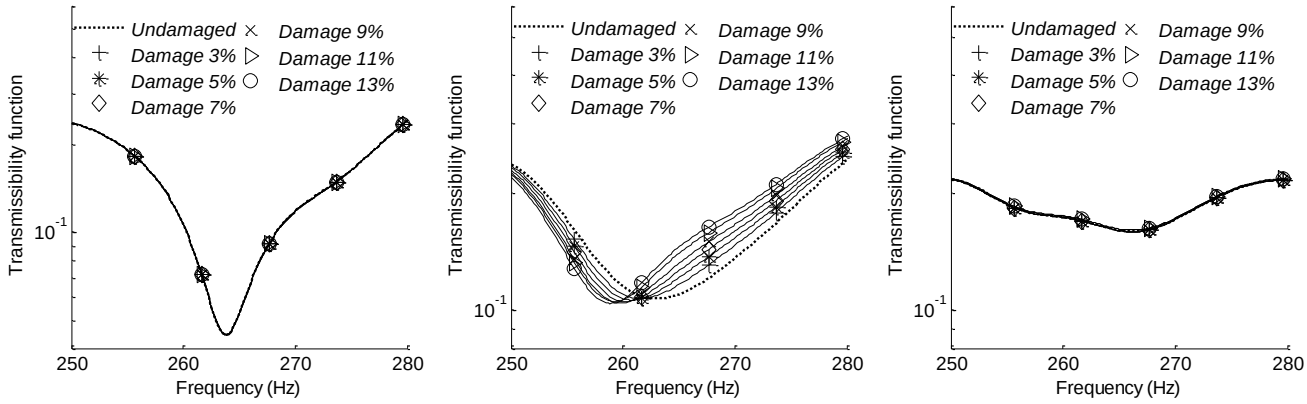

(a) (b) (c)

Fig. 4. Transmissibility functions of different elastic modulus reduction scenarios for location pairs (a) 1-2, (b) 4-5, and (c) 12-13

Damage indicators *TDI* are plotted in Fig. 5 for each damage scenario. The maximum *TDI* occurs exactly at the damage location, even for only 3% elastic modulus reduction. Furthermore, as damage severity increases from 3% to 13%, the value of largest damage indicator increases from 0.0611 to 0.2354. Overall, *TDI* demonstrates both feasibility and accuracy in not only identifying but also locating reduction in elastic modulus.

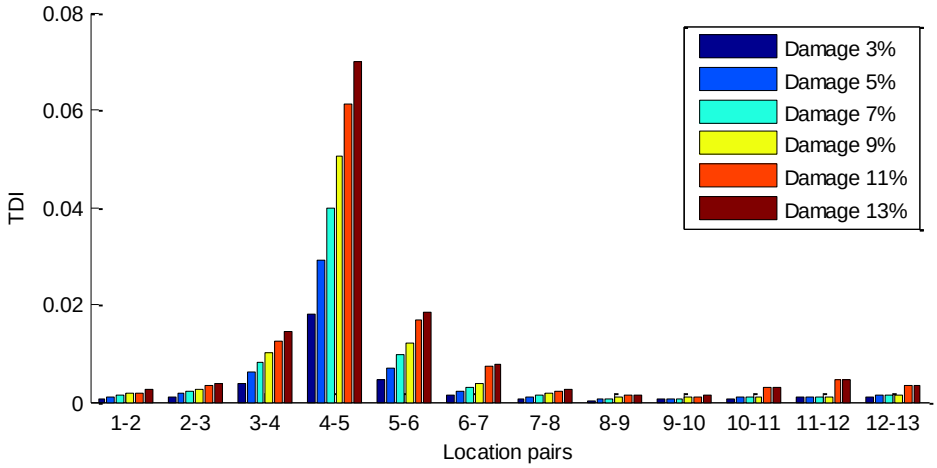

Fig. 5. Transmissibility damage indicators (*TDI*) under different elastic modulus reduction scenarios

4.1.2. Cross correlation analysis

For all different degrees of elastic modulus reduction scenarios, damage detection is performed and the magnitude of cross correlation functions between location pairs 1-2, 4-5, and 12-13 are illustrated in Fig. 6. For clarity, the plots are zoomed in to a smaller time span. Compare with location pairs 1-2 and 12-13, damage-caused change can be observed in cross correlation function at pair 4-5. In addition, for cross correlation functions at pair 4-5, it is obvious that more severe damage causes more change.

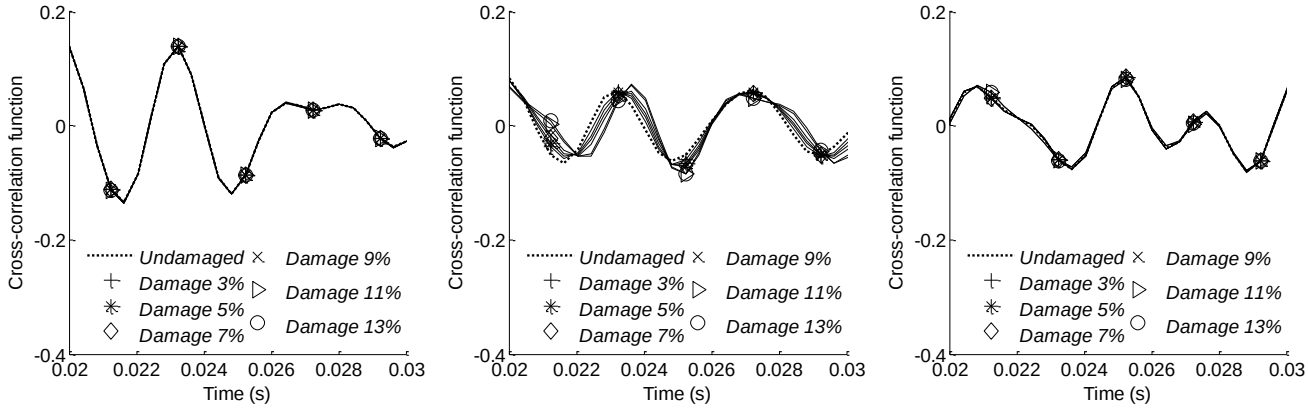

Fig. 6. Cross correlation functions of different elastic modulus reduction scenarios for location pairs (a) 1-2, (b) 4-5, and (c) 12-13

Damage indicator results *CDI* are presented in Fig. 7 for each damage scenario. It can be seen that the damage between locations 4 and 5 is successfully identified in all damage scenarios. For all the damage reduction ratios, the largest damage indicator is clearly at location pair 4-5 and agrees with the correct damage location. Furthermore, as damage severity increases from 3% to 13%, the value of largest damage indicator increases from 0.1276 to 0.4421. Overall, *CDI* demonstrates both feasibility and accuracy in not only identifying but also locating reduction in elastic modulus.

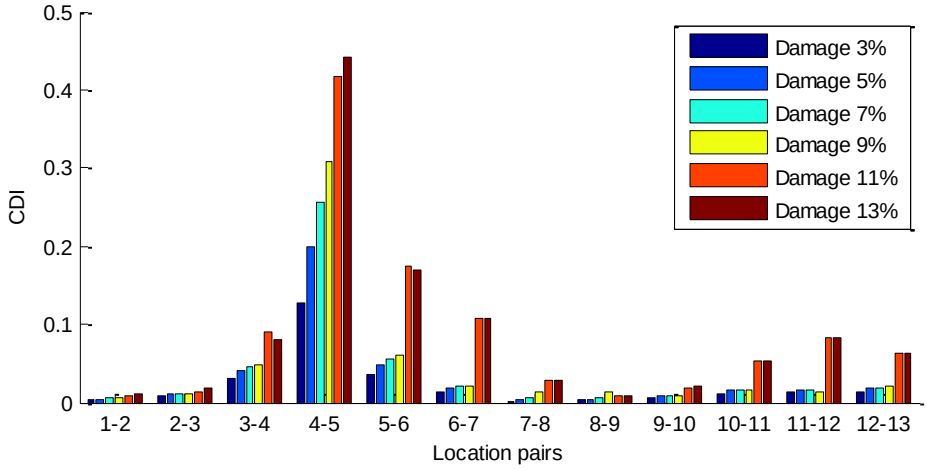

Fig. 7. Cross correlation damage indicators (*CDI*) under different elastic modulus reductions scenarios

4.2. Wall thickness reduction

This section studies the damage detection performance of transmissibility function and cross-correlation algorithm under wall thickness reduction. Wall thickness reduction of the 16-element 2.4m-long ring segment between locations 4 and 5 is first studied. Different degrees of wall thickness reduction are simulated, including 3%, 5%, 7%, 9%, 11%, 13%. The local excitation and measurement schemes remain the same as in Section 4.1.

4.2.1. Transmissibility function

For all different degrees of wall thickness reduction scenarios, the magnitude of transmissibility functions between location pairs 1-2, 4-5, and 12-13 are illustrated in Fig. 8. For clarity, the plots are again zoomed in to a smaller frequency range. Compare with location pairs 1-2 and 12-13, damage-caused change can be observed in transmissibility function at pair 4-5. In addition, for transmissibility function at pair 4-5, it is obvious that more severe damage causes more change.

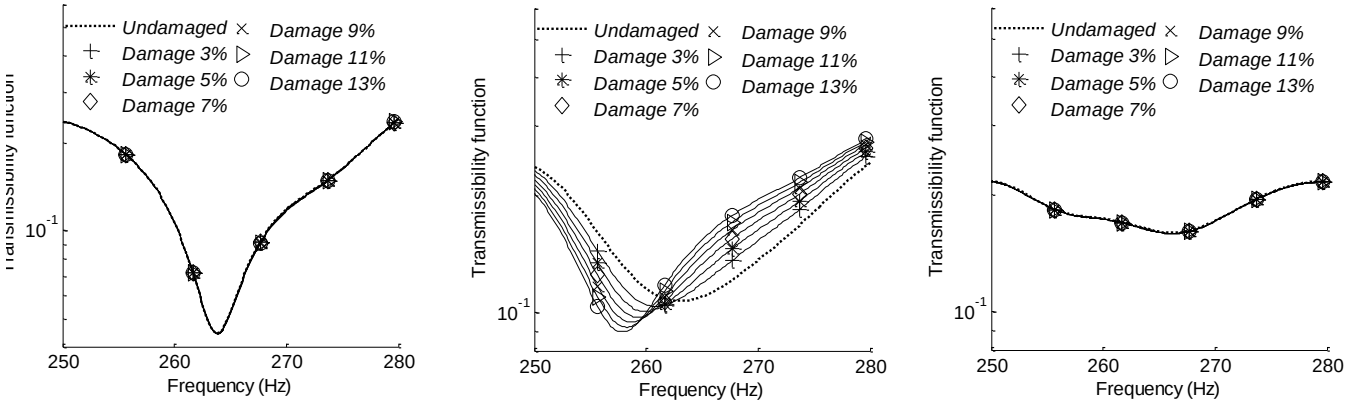

Fig. 8. Transmissibility functions of different wall thickness reduction scenarios for location pairs (a) 1-2, (b) 4-5, and (c) 12-13

Damage indicators *TDI* are plotted in Fig. 9 for each damage scenario. The maximum *TDI* occurs exactly at the damage location, even for only 3% wall thickness reduction. Furthermore, as damage severity increases from 3% to 13%, the value of largest damage indicator increases from 0.0789 to 0.2020. Overall, *TDI* demonstrates both feasibility and accuracy in not only identifying but also locating reduction in wall thickness.

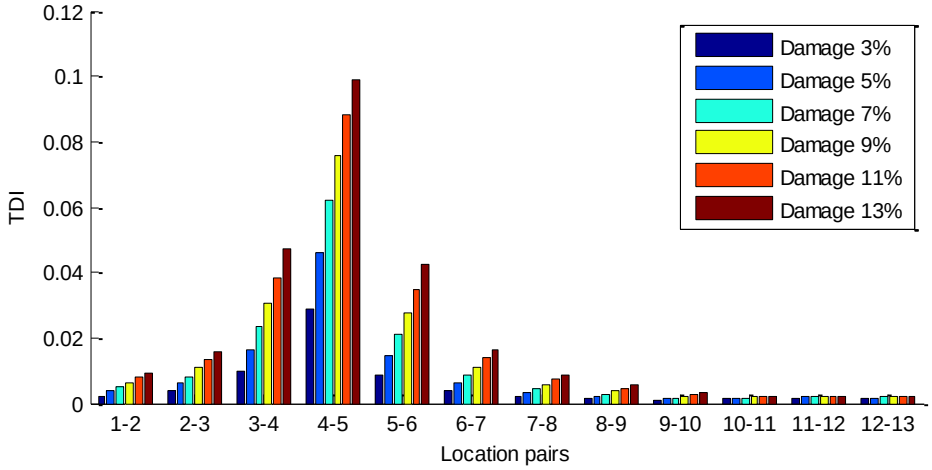

Fig. 9. Transmissibility damage indicators (*TDI*) under wall thickness reduction scenarios

4.2.2. Cross correlation analysis

The magnitude of cross correlation functions between location pairs 1-2, 4-5, and 12-13 are illustrated in Fig. 10, zoomed in to a smaller time span. Compare with location pairs 1-2 and 12-13, damage-caused change can be observed in cross correlation function at pair 4-5. In addition, for cross correlation functions at pair 4-5, it is obvious that more severe damage causes more change.

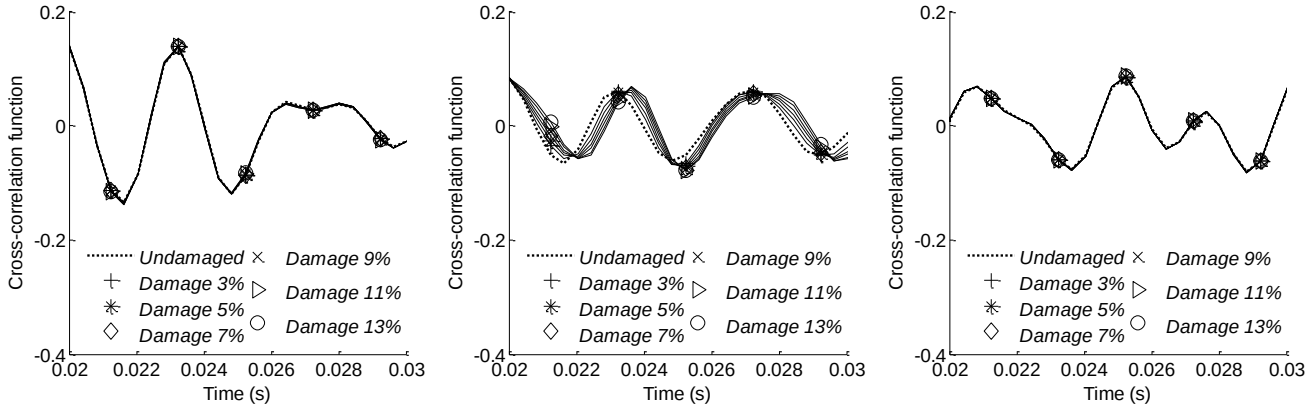

(a) (b) (c)

Fig. 10. Cross correlation functions of different wall thickness reduction scenarios for location pairs (a) 1-2, (b) 4-5, and (c) 12-13

The damage indicators presented in Fig. 11 demonstrate using cross correlation analysis, the damage between locations 4 and 5 can also be identified for all cases. The maximum *CDI* occurs exactly at the damage location, even for only 3% elastic modulus reduction. Furthermore, as damage severity increases from 3% to 13%, the value of largest damage indicator increases from 0.1661 to 0.4161. Overall, *CDI* demonstrates both feasibility and accuracy in not only identifying but also locating reduction in wall thickness.

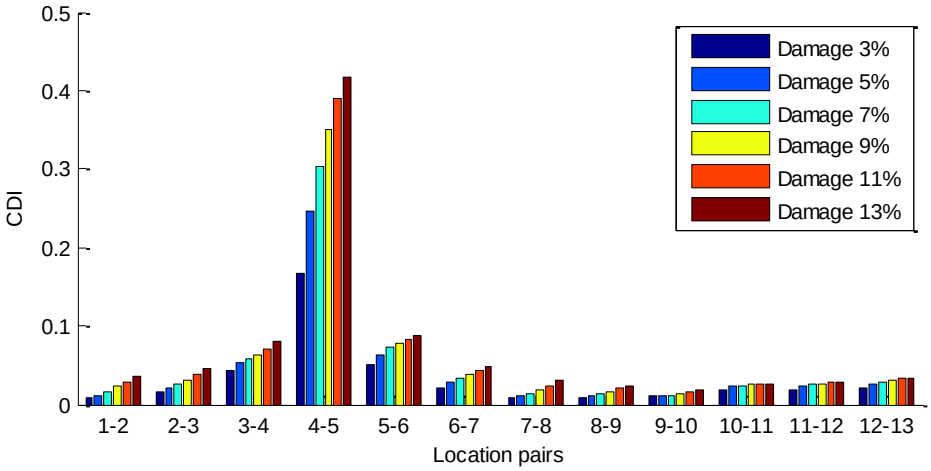

Fig. 11. Cross correlation damage indicators (*CDI*) under different wall thickness reduction scenarios

4.3. Two damage locations with same damage type

In this subsection, two damage locations with same damage types are studied. The first damage location occurs at the 16-element 2.4m-long ring segment between locations 4 and 5, and the second damage location occurs at the 2.4m-long ring segment between locations 8 and 9, elastic modulus reduction of 7% is applied to both damage locations, as shown in Fig. 2.

4.3.1. Transmissibility function

The local excitation and measurement schemes remain the same as in Section 4.1. Comparison of transmissibility functions between location pairs 1-2, 4-5, 7-8, and 12-13 for two-damage model is presented in Fig. 12. It is observed that transmissibility functions close to the damage locations demonstrate larger difference between undamaged and damaged structures. Among all four location pairs, larger change occurs at pair 4-5 and pair 8-9.

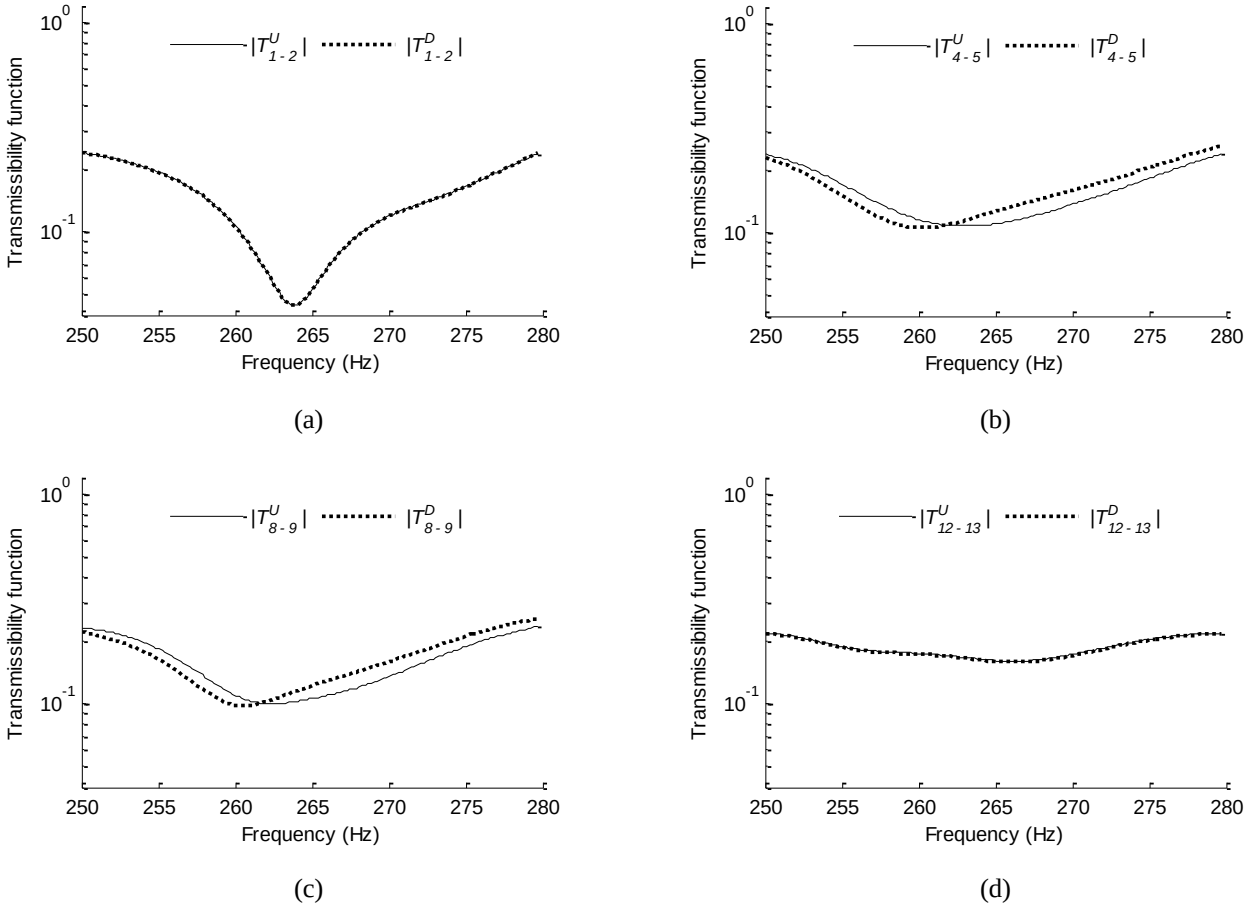

Fig. 12. Comparison of transmissibility functions of two damage locations with same damage type: (a) 1-2, (b) 4-5, (c) 8-9, and (d) 12-13

Damage indicators *TDI* for all twelve location pairs are shown in Fig. 13. As expected, the larger *TDI* values occur exactly at the damage location, both two damage locations can be accurately identified by the transmissibility-function based damage indictor.

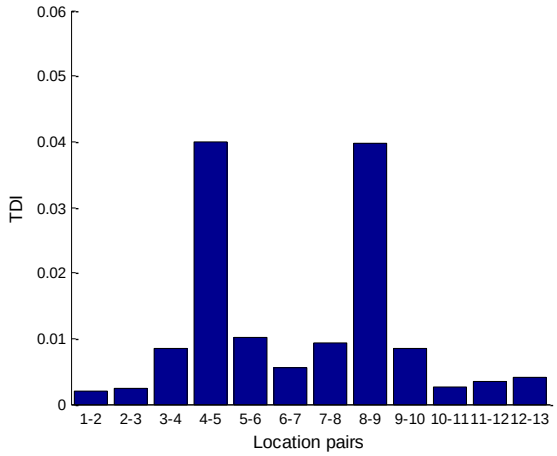

Fig. 13. Transmissibility damage indicators (*TDI*) under two damage locations with same damage type

4.3.2. Cross correlation analysis

Using same excitation and measurement scheme for data collection, comparison of cross correlation function between location pairs 1-2, 4-5, 7-8, and 12-13 for two-damage model is presented in Fig. 14. Among all four location pairs, larger change occurs at pair 4-5 and pair 8-9.

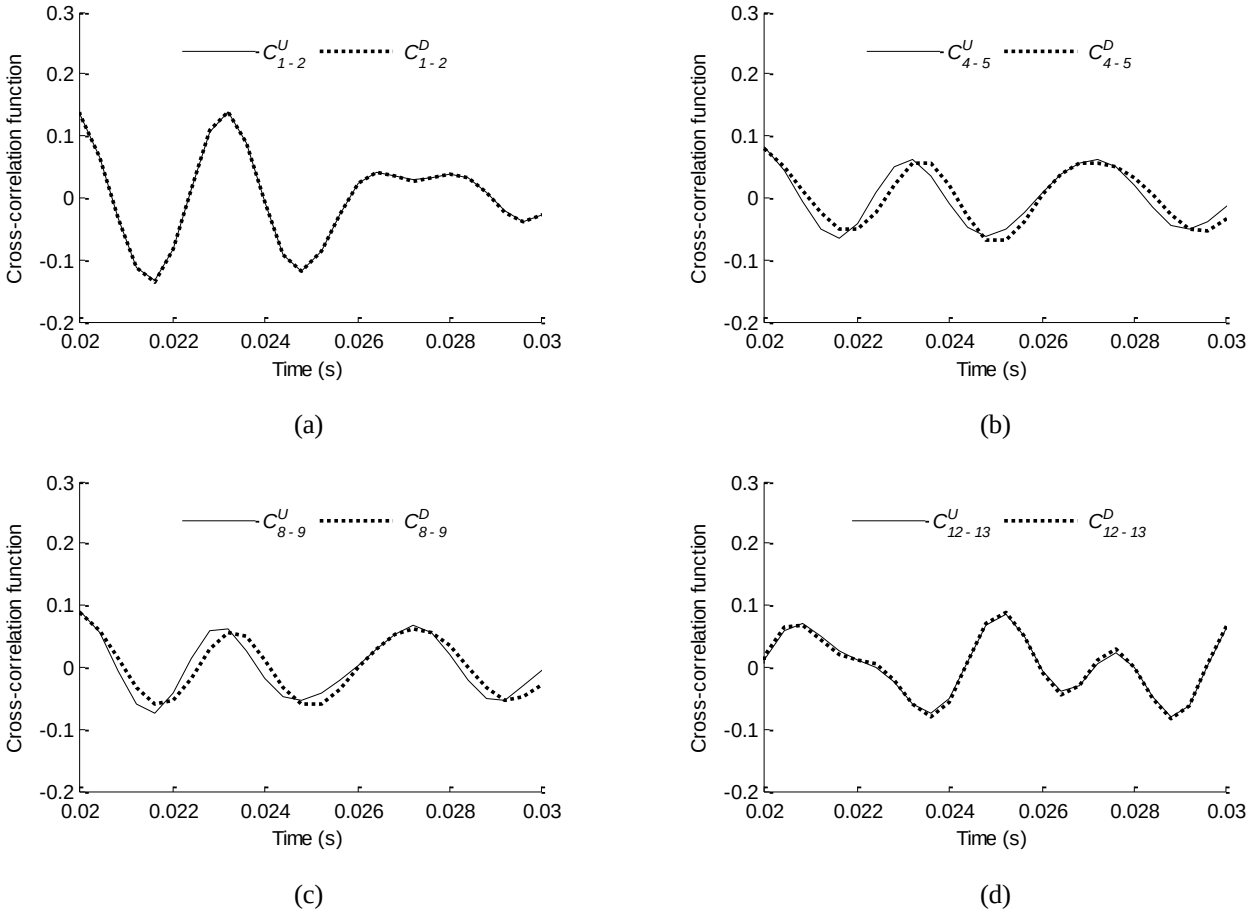

Fig. 14. Comparison of cross correlations of two damage locations with same damage type: (a) 1-2, (b) 4-5, (c) 8-9, and (d) 12-13

Cross correlation damage indicators (*CDI*) are shown in Fig. 15. The results demonstrate that both damage locations (the first between locations 4 and 5; the second between locations 8 and 9) can be identified successfully.

4.4. Two damage locations with different damage types

This subsection studies the scenario when two different types of damage occur (Fig. 2). At the first damage between locations 4 and 5, elastic modulus reduction of 7% is again applied to two adjacent ring segments of 16 tunnel wall elements. At the second damage between locations 8 and 9, wall thickness reduction of 7% is applied to two adjacent ring segments. The local excitation and measurement schemes remain the same as in Section 4.1.

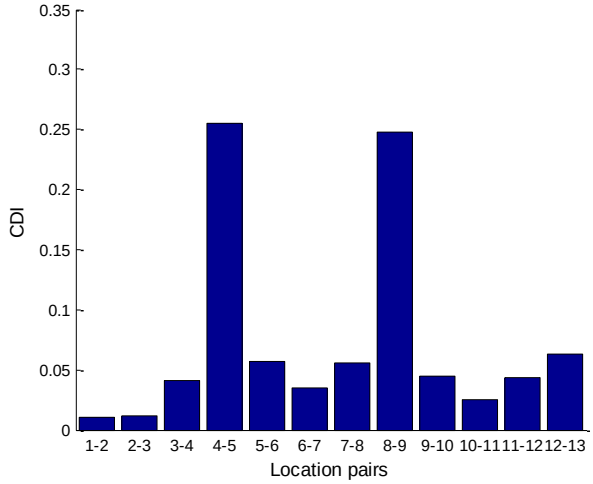

Fig. 15. Cross correlation damage indicators (*CDI*) under two damage locations with same damage type

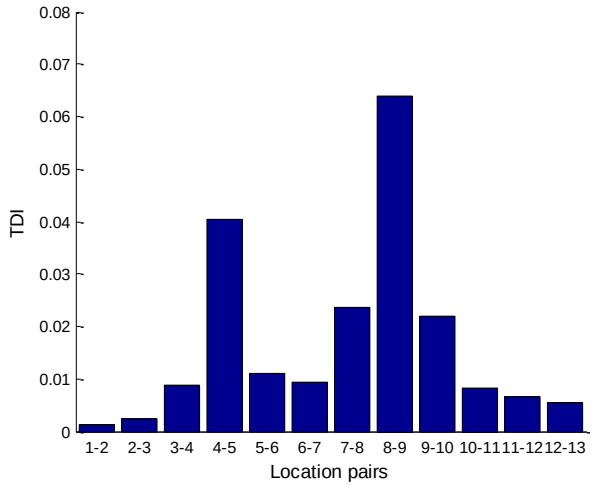

Fig. 16. Transmissibility damage indicators (*TDI*) under two damage locations with different damage types

4.4.1. Transmissibility function

Similar as previously, transmissibility function damage indicators *TDI* for twelve pairs of measurement locations are shown in Fig. 16. It is observed that although damage types are different, both damage locations can be identified by the damage indictor. In addition, the indicator value at wall thickness reduction is larger than the value at elastic modulus reduction. Both elastic modulus reduction and wall thickness reduction are essentially reducing structural stiffness. However, elastic modulus reduction changes structural stiffness linearly, yet wall thickness reduction changes structural geometry and affects structural stiffness exponentially. Therefore, wall thickness change generates larger effect on structural dynamic properties than stiffness change.

4.4.2. Cross correlation analysis

Cross-correlation damage indicators (*CDI*) are calculated for this scenario and plotted in Fig. 17. It is shown that damage indicators close to the actual damage locations are obviously larger than other locations. Both damage locations can be identified, while the damage indicator value for wall thickness reduction is larger than the value for elastic modulus reduction. As elucidated before, wall thickness change is not only affect the stiffness, but also decrease the structural geometry and mass. The wall thickness change gives larger influence to structural properties than elastic modulus change.

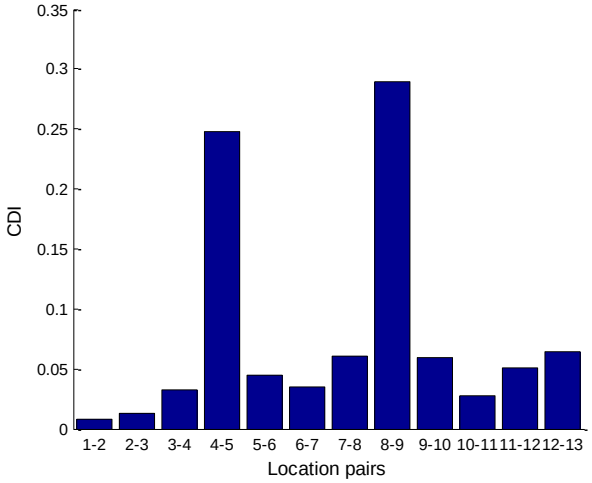

Fig. 17. Cross correlation damage indicators (*CDI*) of two damage locations with different damage types

4.5. Damage detection results under different noise levels

This section studies the damage detection performance of transmissibility function and cross-correlation algorithm under various noise levels. Wall thickness reduction of 7% is applied to the 16-element 2.4m-long ring segment between locations 4 and 5. Different levels of Gaussian noise is introduced to the original acceleration data; then the damage detection procedure is carried out as before. Three different noise-to-signal levels (0.1%, 1%, and 3%) are studied, i.e. corresponding signal-to-noise ratios (SNR) are 30dB, 20dB, 15dB. The local excitation and measurement schemes remain the same as in Section 4.1.

4.5.1. Transmissibility function

Fig. 18 presents the transmissibility functions under different noise levels (no noise, 0.1%, 1%, and 3% noise). Slight fluctuations appear on transmissibility function curves when noise is introduced. The fluctuation amplitude grows with the increase of noise level, which makes it difficult to visually distinguish change caused by structural damage.

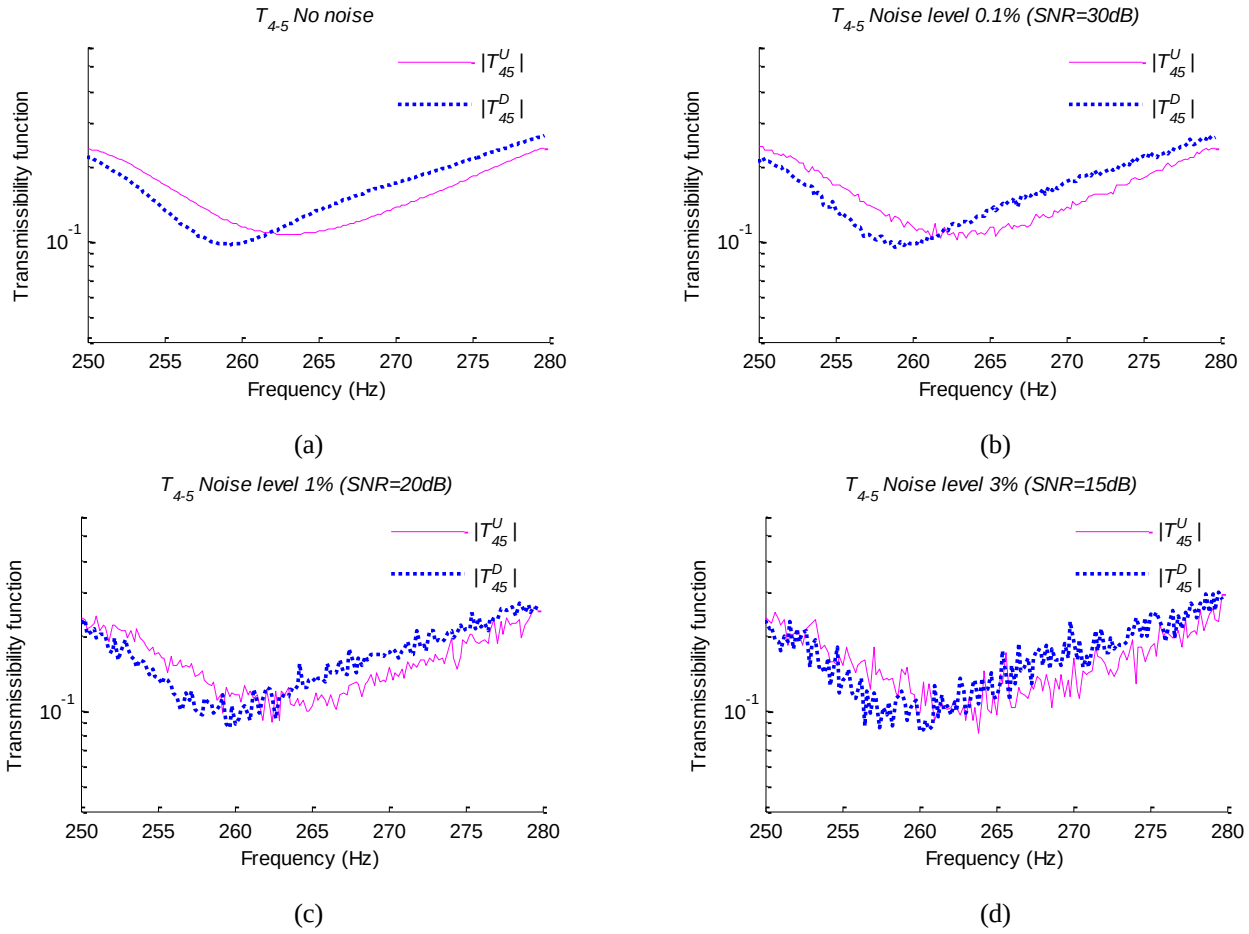

Fig. 18. Comparison of transmissibility functions under different noise levels: (a) no noise; (b) 0.1% noise; (c) 1% noise; (d) 3% noise.

Transmissibility function damage indicators *TDI* under different noise levels are shown in Fig. 19. Damage locations can still be accurately identified by the transmissibility-function based damage indictor for all noise levels. However, it can be observed that the difference of *TDI* values between a damage location and an undamaged location decreases as noise level increases.

4.5.2. Cross correlation analysis

Fig. 20 presents the entire time span of cross correlation functions under different noise levels. Differences appear at both ends of the cross correlation curve when Gaussian noise is introduced. The difference increases with an increasing noise level. According to Eq. (9), cross correlation values around time zero are calculated by averaging the products of more data points, thus, the influence of Gaussian noise is significantly reduced. Meanwhile, at two ends of the time axis, cross correlation values are calculated by averaging the products of fewer data points, where the influence of Gaussian noise cannot be neglected.

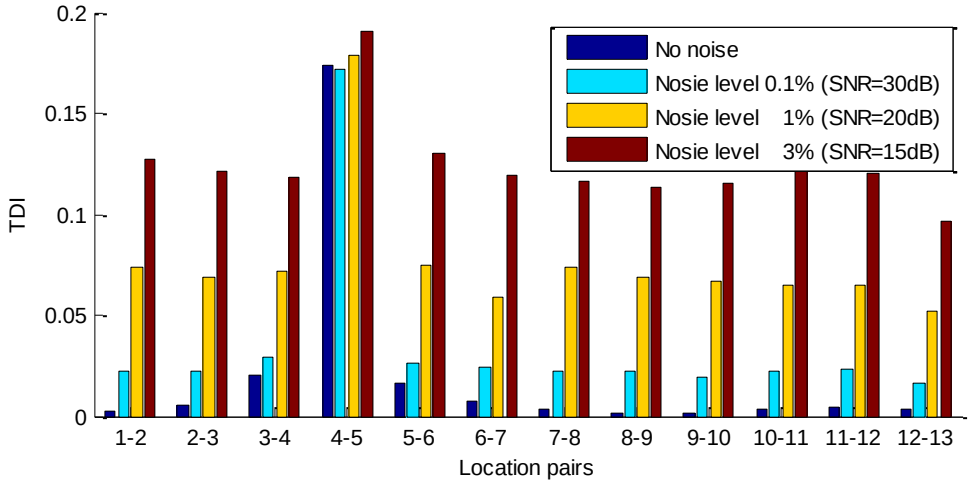

Fig. 19. Transmissibility damage indicators (*TDI*) under different noise levels

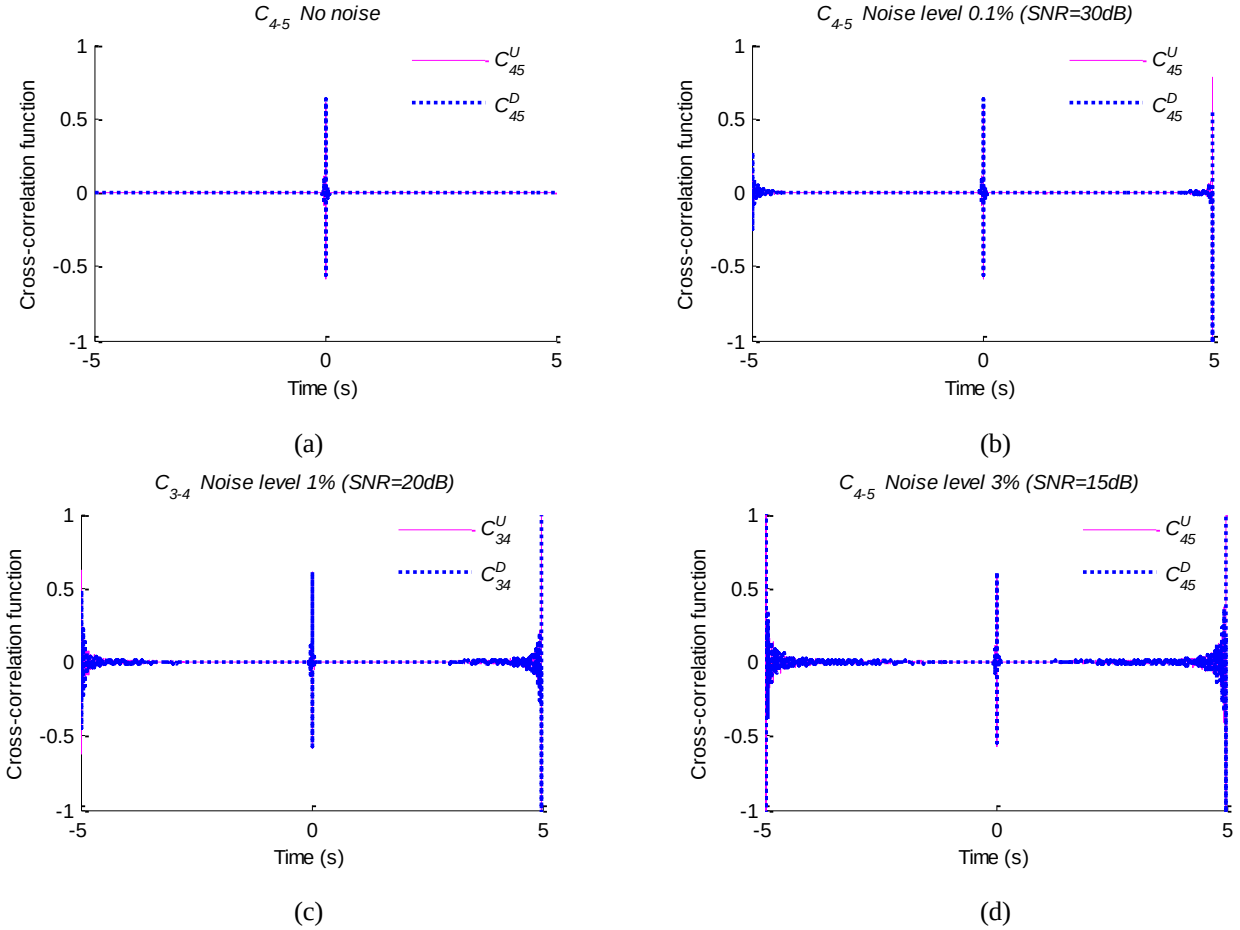

Fig. 20. Comparison of cross correlation functions under different noise levels (entire time span): (a) no noise; (b) 0.1% noise; (c) 1% noise; (d) 3% noise.

The cross correlation curves are magnified around time zero and presented in Fig. 21. It can be confirmed that values around time zero are almost not affected by noise. The values remain almost constant for all noise levels.

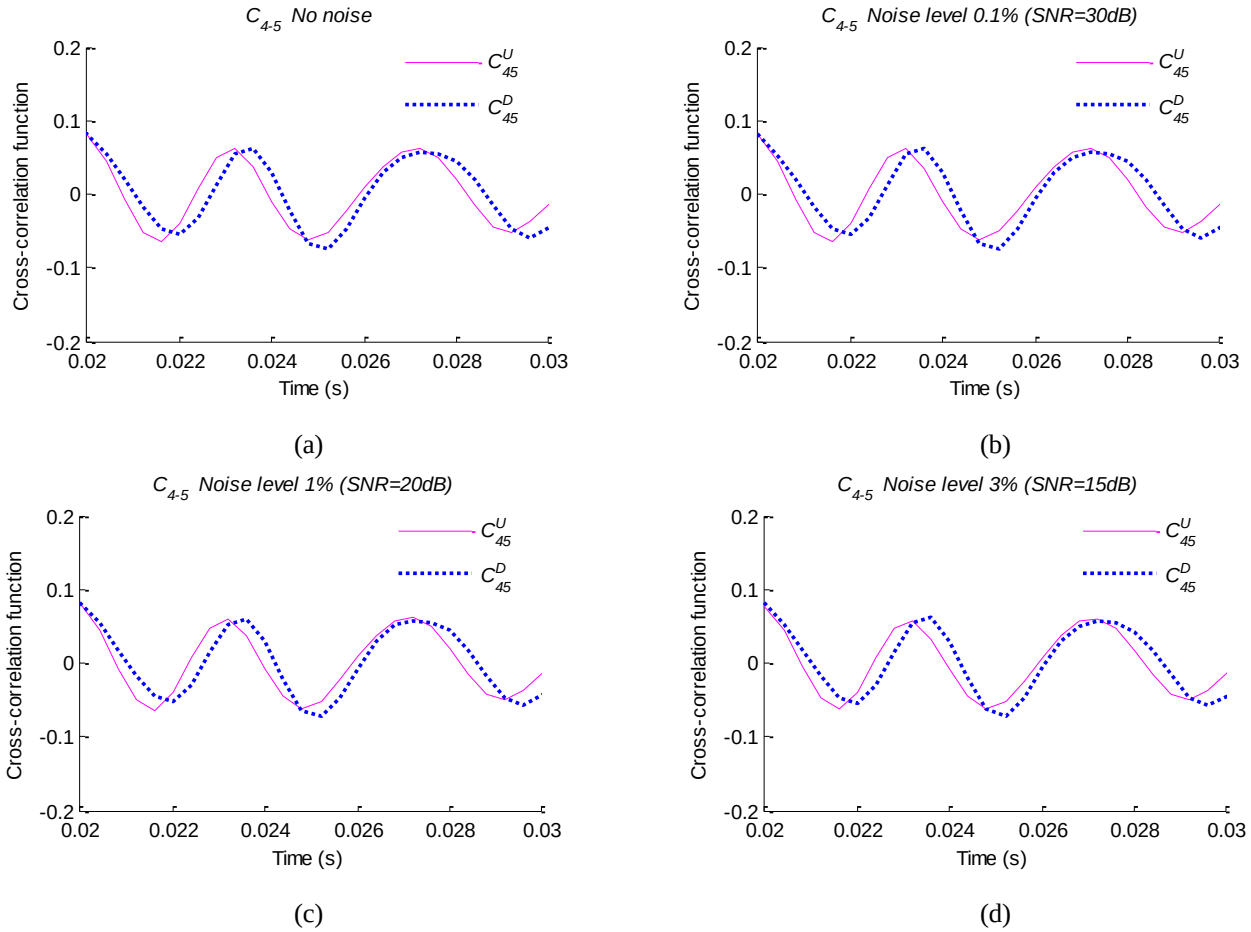

Fig. 21. Comparison of cross correlation functions under different noise levels (zoom-in): (a) no noise; (b) 0.1% noise; (c) 1% noise; (d) 3% noise.

Cross correlation damage indicators *CDI* under different noise levels are calculated by using time span -0.03s ~ +0.03s and presented in Fig. 22. Damage locations can be accurately identified by the cross-correlation based indictor, for all noise levels. Cross correlation algorithm demonstrates better robustness against sensor noise.

5. Discussion

With the proposed measurement and excitation scheme, results of Section 4 shown that both transmissibility function and cross correlation algorithms can be used for detecting different types of damage. Both algorithms give reliable damage identification results when either elastic modulus reduction or wall thickness reduction occurs.

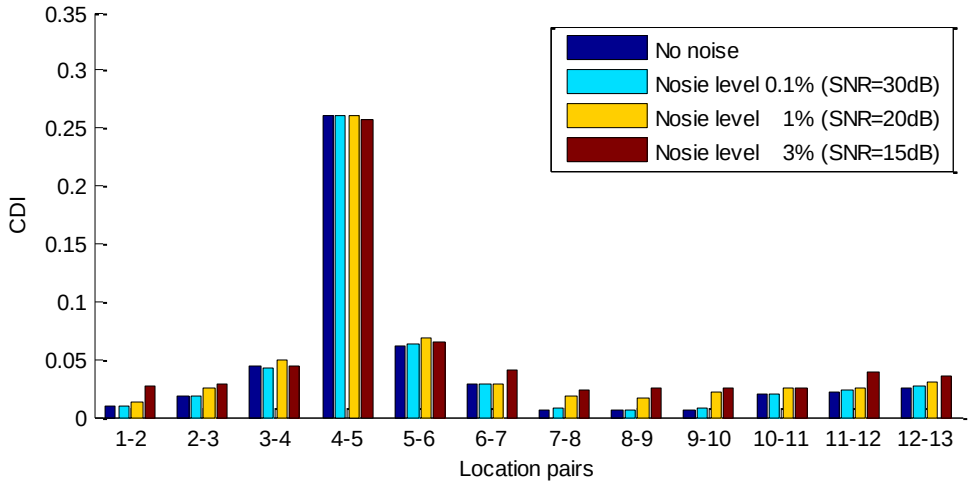

Fig. 22. Cross correlation damage indicators (*CDI*) under different noise levels

As the ratio between two entries of structural transfer function matrix, transmissibility functions directly reflect inherent dynamic structural properties. It is found that once an appropriate frequency range is selected, stable damage detection results can be acquired through transmissibility function analysis. Meanwhile, cross correlation algorithm offers of the convenience of directly processing time domain signal, without the requirement of appropriately selecting frequency range. This property makes the cross correlation algorithm easy to implementation. On the other hand, it should be realized that cross correlation analysis is usually not as sensitive to damage types as transmissibility function. The previous results with multiple damage scenarios demonstrate that when two similar damage types are simultaneously introduced into the tunnel model, the transmissibility function algorithm can give the same *TDI* values, but different *CDI* values may be acquired by the cross correlation algorithm. Also, when two different damage types are introduced, the difference in the two *TDI* values was shown to be larger than the difference in the two *CDI* values. In other words, transmissibility function algorithm is more sensitive to damage types than cross correlation analysis, and has the ability of distinguishing different damage types. On the other hand, the simulations with sensor noise shows cross correlation algorithm demonstrates better robustness against sensor noise. Nevertheless, the practical experimental environment can be much more complex, and the damage detection performance is to be verified in future field tests.

6. Conclusions

This paper investigates the application of two damage detection and localization approaches, i.e. transmissibility function and cross correlation analysis, in metro tunnel engineering. A finite element tunnel model for one segment of Shanghai metro rail system is constructed with soil constraints. The feasibility and sensitivity of proposed approaches have been validated for different damage scenarios. Furthermore, the proposed experimental strategies represent localized schemes for excitation and

measurement, where only a few vibration measurements very close to the impact excitation are needed. This local excitation and measurement schemes provides great convenience in field implementation. Nevertheless, this study also discovers that each approach has its own limitation. Because both algorithms have advantages and disadvantages, and they can be adopted in combination to cross check the damage identification results.

Experimental validation of the damage detection algorithms can be conducted in the future. Transmissibility function and cross correlation algorithm under random excitation input could be investigated, which can make these methodologies more useful for practical applications. Furthermore, wireless sensor network (WSN) technology provides a promising approach to monitor metro tunnel structures. Wireless sensor networks have advantages in cost, size, flexibility, and distributed intelligence, when compared with traditional cabled monitoring. Both transmissibility function and cross correlation algorithms are simple and easy to implement on a wireless sensing unit. The onboard computing and storage capacity of wireless sensing units make them attractive in detecting and localizing damage in a decentralized fashion.

Acknowledgement

This work is funded by National Basic Research Program of China (973 Program: 2011CB013800), National Natural Science Founds of China (41372273) and Shanghai Science and Technology Development Funds (12231200900, 13231200100). This research is also partially sponsored by the U.S. National Science Foundation, under grant numbers CMMI-1150700 and CMMI-1041607. Any opinions, findings, and conclusions or recommendations expressed in this material are those of the authors and do not necessarily reflect the views of the National Science Foundation.

References

[1] Stajano, F., N. Hoult, I. Wassell, P. Bennett, C. Middleton, and K. Soga, Smart bridges, smart tunnels: Transforming wireless sensor networks from research prototypes into robust engineering infrastructure, Ad Hoc Networks. 8 (8) (2010) 872-888.

[2] Bennett, P.J., K. Soga, I. Wassell, P. Fidler, K. Abe, Y. Kobayashi, and M. Vanicek, Wireless sensor networks for underground railway applications: case studies in Prague and London, Smart Structures and Systems. 6 (5-6) (2010) 619-639.

[3] Doebling, S.W., C.R. Farrar, M.B. Prime, D.W. Shevitz, Damage identification and health monitoring of structural and mechanical systems from changes in their vibration characteristics: a literature review, Los Alamos National Lab, NM (United States), 1996.

[4] Doebling, S.W., C.R. Farrar, M.B. Prime, A summary review of vibration-based damage identification methods, Shock and vibration digest. 30 (2) (1998) 91-105.

[5] Chesné, S., A. Deraemaeker, Damage localization using transmissibility functions: a critical review, Mechanical Systems and Signal Processing. 38 (2) (2013) 569-584.

[6] Zhou, B., X.Y. Xie, Y.B. Yang, J.C. Jiang, A novel vibration-based structure health monitoring approach for the shallow buried tunnel, Computer Modeling in Engineering & Sciences(CMES). 86 (4) (2012) 321-348.

[7] Zhou, B., X. Xie, Y. Li, A structural health assessment method for shield tunnels based on torsional wave speed, Science China Technological Sciences. 57 (6) (2014) 1109-1120.
[8] Liu, W., D. Ewins, Transmissibility properties of MDOF systems, in: Proceedings of the 16th international modal analysis conference, California, USA, 1998, pp. 847-854.
[9] Ribeiro, A., J. Silva, N. Maia, On the generalisation of the transmissibility concept, Mechanical Systems and Signal Processing. 14 (1) (2000) 29-35.
[10] Zhang, H., M. Schulz, A. Naser, F. Ferguson, P. Pai, Structural health monitoring using transmittance functions, Mechanical Systems and Signal Processing. 13 (5) (1999) 765-787.
[11] Johnson, T.J., D.E. Adams, Transmissibility as a differential indicator of structural damage, Journal of vibration and acoustics. 124 (4) (2002) 634-641.
[12] Johnson, T.J., R.L. Brown, D.E. Adams, M. Schiefer, Distributed structural health monitoring with a smart sensor array, Mechanical Systems and Signal Processing. 18 (3) (2004) 555-572.
[13] Caccese, V., R. Mewer, S.S. Vel, Detection of bolt load loss in hybrid composite/metal bolted connections, Engineering structures. 26 (7) (2004) 895-906.
[14] Kess, H., D. Adams, Investigation of operational and environmental variability effects on damage detection algorithms in a woven composite plate, Mechanical Systems and Signal Processing. 21 (6) (2007) 2394-2405.
[15] Yi, X., D. Zhu, Y. Wang, J. Guo, K.-M. Lee, Embedded transmissibility function analysis for damage detection in a mobile sensor network, in: Proceedings of SPIE Conference on Smart Structures and Materials+ Nondestructive Evaluation and Health Monitoring, California, USA, 2010.
[16] Zhu, D., X. Yi, Y. Wang, K.-M. Lee, J. Guo, A mobile sensing system for structural health monitoring: design and validation, Smart materials and structures. 19 (5) (2010) 055011.
[17] Farrar, C., G. James III, System identification from ambient vibration measurements on a bridge, Journal of sound and vibration. 205 (1) (1997) 1-18.
[18] Lin, S., J.N. Yang, L. Zhou, Damage identification of a benchmark building for structural health monitoring, Smart materials and structures. 14 (3) (2005) S162-S169.
[19] Zhu, D., X. Yi, Y. Wang, K.G. Sabra, Structural damage detection through cross correlation analysis of mobile sensing data, in: Proceedings of the 5th World Conference on Structural Control and Monitoring, Tokyo, Japan, 2010.
[20] Heckman, V., M. Kohler, T. Heaton, A damage detection method for instrumented civil structures using prerecorded green's functions and cross-correlation, in: The 6th International Workshop on Advanced Smart Materials and Smart Structures Technology, Dalian, China, 2011.
[21] Wood, A.M., The circular tunnel in elastic ground, Geotechnique. 25 (1) (1975) 115-127.
[22] Huang, M., J. Cao, Simplified analysis of tunnel earthquake response and centrifuge modelling calibration, Chinese Journal of Rock Mechanics and Engineering. 29 (2) (2010) 271-280.